U-Load Dextramer®
Build multimers with your choice of peptide and peptide-receptive MHC I and MHC II alleles.

The Journal of Immunology

This information is current as of February 24, 2022.

The Lysophosphatidylcholine Transporter MFSD2A Is Essential for CD8 $^{+}$ Memory T Cell Maintenance and Secondary Response to Infection

Ann R. Piccirillo, Eric J. Hyzny, Lisa Y. Beppu, Ashley V. Menk, Callen T. Wallace, William F. Hawse, Heather M. Buechel, Bernice H. Wong, Juat Chin Foo, Amaury Cazenave-Gassiot, Markus R. Wenk, Greg M. Delgoffe, Simon C. Watkins, David L. Silver and Louise M. D'Cruz

J Immunol 2019; 203:117-126; Prepublished online 24 May 2019;
doi: 10.4049/jimmunol.1801585
http://www.jimmunol.org/content/203/1/117

Supplementary Material **http://www.jimmunol.org/content/suppl/2019/05/23/jimmunol.1801585.DCSupplemental**

References This article **cites 40 articles**, 12 of which you can access for free at:
http://www.jimmunol.org/content/203/1/117.full#ref-list-1

Why *The JI*? Submit online.

- **Rapid Reviews! 30 days*** from submission to initial decision
- **No Triage!** Every submission reviewed by practicing scientists
- **Fast Publication!** 4 weeks from acceptance to publication

**average*

Subscription Information about subscribing to *The Journal of Immunology* is online at:
http://jimmunol.org/subscription

Permissions Submit copyright permission requests at:
http://www.aai.org/About/Publications/JI/copyright.html

Email Alerts Receive free email-alerts when new articles cite this article. Sign up at:
http://jimmunol.org/alerts

The Journal of Immunology is published twice each month by
The American Association of Immunologists, Inc.,
1451 Rockville Pike, Suite 650, Rockville, MD 20852
Copyright © 2019 by The American Association of Immunologists, Inc. All rights reserved.
Print ISSN: 0022-1767 Online ISSN: 1550-6606.

Downloaded from http://www.jimmunol.org/ by guest on February 24, 2022

The Lysophosphatidylcholine Transporter MFSD2A Is Essential for CD8$^+$ Memory T Cell Maintenance and Secondary Response to Infection

Ann R. Piccirillo,* Eric J. Hyzny,* Lisa Y. Beppu,* Ashley V. Menk,† Callen T. Wallace,‡ William F. Hawse,* Heather M. Buechel,* Bernice H. Wong,§ Juat Chin Foo,¶ Amaury Cazenave-Gassiot,¶ Markus R. Wenk,¶ Greg M. Delgoffe,† Simon C. Watkins,‡ David L. Silver,§ and Louise M. D'Cruz*

Access to nutrients is critical for an effective T cell immune response to infection. Although transporters for sugars and amino acids have previously been described in the context of the CD8$^+$ T cell immune response, the active transport of exogenous fatty acids has remained enigmatic. In this study, we discovered that the sodium-dependent lysophosphatidylcholine (LPC) transporter major facilitator superfamily domain containing 2A (MFSD2A) is upregulated on activated CD8$^+$ T cells and is required for memory T cell maintenance. MFSD2A deficiency in mice resulted in decreased import of LPC esterified to long chain fatty acids into activated CD8$^+$ T cells, and MFSD2A-deficient cells are at a competitive disadvantage resulting in reduced memory T cell formation and maintenance and reduced response to secondary infection. Mechanistically, import of LPCs was required to maintain T cell homeostatic turnover, which when lost resulted in a decreased memory T cell pool and thus a reduced secondary response to repeat infection. ***The Journal of Immunology*****, 2019, 203: 117–126.**

The CD8$^+$ T cell immune response affords both effector function to kill infected cells and long-lasting protective memory against a wide variety of immunological insults (1). It is now known that effector and memory CD8$^+$ T cells dramatically alter their metabolic programs upon activation and differentiation, changing from quiescent naive cells that rely primarily on oxidative phosphorylation (OXPHOS) to effector T cells that engage aerobic glycolysis before establishment and maintenance of memory requiring OXPHOS and lipolysis (2–4). A number of pioneering studies have described how effector and memory T cells acquire external metabolites such as glycerol, glucose, and neutral amino acids to fuel their metabolic requirements after activation (5–7). Additionally, multiple studies have focused on how fatty acid synthesis and fatty acid oxidation are regulated in effector and memory T cells (3, 4, 8–13). Recent new data have shown that memory T cell formation is, in fact, independent of fatty acid oxidation and have instead suggested that other metabolic pathways must be required for differentiation and maintenance of memory CD8$^+$ T cells (14). Moreover, these new data suggest that exogenous long chain fatty acid (LCFAs) may be used for biosynthesis and for biomass generation (14). Currently, little evidence exists for how exogenous lipids might affect the CD8$^+$ effector T cell response and whether specific mechanisms exist for the import of exogenous fatty acids into effector T cells.

The major facilitator superfamily domain containing 2A (MFSD2A) protein was, until recently, considered an orphan transporter, upregulated during fasting, and controlled by expression of PPARα and glucagon signaling in the liver (15). New evidence for the function of MFSD2A has been uncovered, detailing a requirement for MFSD2A at the blood–brain barrier (BBB) (16). MFSD2A is essential for the maintenance of the BBB and, importantly, for transport of ω-3 LCFAs, including docosahexaenoic acid (DHA), across the BBB and blood–retinal barrier and into the eye and brain (16, 17). LCFAs are transported esterified to the phospholipid lysophosphatidylcholine (LPC) by MFSD2A (16, 17). In humans, identification of individuals with mutations in conserved residues of MFSD2A were identified, and these patients have severe problems with brain growth and development (18–20). More recently it has been shown that loss of MFSD2A at the BBB results in increased de novo fatty acid lipogenesis, a

*Department of Immunology, University of Pittsburgh, Pittsburgh, PA 15213; †Tumor Microenvironment Center, UPMC Hillman Cancer Center, Pittsburgh, PA 15232; ‡Center for Biologic Imaging, University of Pittsburgh, Pittsburgh, PA 15213; §Signature Research Program in Cardiovascular and Metabolic Diseases, Duke-National University of Singapore Graduate Medical School, Singapore 159857, Singapore; and ¶Department of Biochemistry, National University of Singapore, Singapore 117597, Singapore

ORCIDs: 0000-0002-4141-3050 (E.J.H.); 0000-0002-6918-1159 (L.Y.B.); 0000-0001-8371-3345 (W.F.H.); 0000-0002-0955-200X (H.M.B.); 0000-0001-8981-1376 (B.H.W.); 0000-0002-9189-4585 (J.C.F.); 0000-0002-3050-634X (A.C.-G.); 0000-0003-4092-1552 (S.C.W.); 0000-0003-0388-430X (L.M.D.).

Received for publication December 4, 2018. Accepted for publication April 29, 2019.

This work was supported by the National Institutes of Health (NIH) R21AI135238 (to L.M.D.) and seed funding from the University of Pittsburgh (to W.F.H. and L.M.D.), NIH DP2AI136598 (to G.M.D.), and the National Research Foundation Singapore (https://www.nrf.gov.sg) (Grants NRFI2017-05 to D.L.S. and NRFI2015-05) to M.R.W.).

A.R.P., L.Y.B., H.M.B., and W.F.H. designed and performed experiments. E.J.H., C.T.W., and S.C.W. were responsible for generating and analyzing the confocal microscopy data. A.V.M. and G.M.D. generated the Seahorse data. B.H.W., J.C.F., A.C.-G., and M.R.W. performed and generated the mass spectrometry lipidomics experiments and analysis. D.L.S. generated the MFSD2A conditional mice, provided the mass spectrometry lipidomics data, and provided intellectual insight. L.M.D. designed the experiments and wrote the manuscript.

Address correspondence and reprint requests to Louise M. D'Cruz, University of Pittsburgh, Department of Immunology, Biomedical Science Tower, 200 Lothrop Street, Pittsburgh, PA 15213. E-mail address: ldcruz@pitt.edu

The online version of this article contains supplemental material.

Abbreviations used in this article: AQP9, aquaporin 9; BBB, blood–brain barrier; DHA, docosahexaenoic acid; ECAR, extracellular acidification rate; HILIC, hydrophilic interaction liquid chromatography; LCFA, long chain fatty acid; LPC, lysophosphatidylcholine; MFI, median fluorescence intensity; MFSD2A, major facilitator superfamily domain containing 2A; OCR, oxygen consumption rate; OXPHOS, oxidative phosphorylation; PC, phosphatidylcholine; SRC, spare respiratory capacity; SREBP, sterol regulatory element binding protein; WT, wild-type.

Copyright © 2019 by The American Association of Immunologists, Inc. 0022-1767/19/$37.50

www.jimmunol.org/cgi/doi/10.4049/jimmunol.1801585

Downloaded from http://www.jimmunol.org/ by guest on February 24, 2022

compensatory mechanism for loss of DHA, which was regulated by the sterol regulatory element binding proteins (SREBPs) (21).

The main organ that produces LPC is the liver, although the enzymes that are responsible for LPC generation in the liver have not yet been identified (22–25). Plasma LPC can transport esterified fatty acids, phosphatidylcholine (PC), and glycerol between tissues (24), and once transferred across the plasma membrane and into the cytoplasm, LPC can be processed into multiple products such as PC, phosphatidic acid, diacylglycerol (DAG), and triglycerides (24). In plasma, the most common LCFAs esterified to LPC are palmitate and stearate, with DHA found at relatively low levels (16).

Current research into metabolism during the effector T cell immune response has focused on how these cells use metabolites within the cell to affect metabolic changes and modulate energy expenditure as necessary (2, 3, 11, 26). A number of studies have investigated how activated T cells incorporate exogenous glycerol (using aquaporin 9; AQP9) (5), glucose (using GLUT1) (6, 27), and neutral amino acids (using Slc7a5) (7) to be used as potential fuel sources for the synthesis of triacylglycerides and ATP (5, 6, 27) and for activation of mTORC1 and expression of c-Myc (7). However, there is currently very little understood about the processes by which effector T cells transport exogenous phospholipids such as esterified LPC species across their cell membrane (28) or how loss of these LPCs might perturb effector and memory T cell biology. A number of studies have previously attempted to address this, but caveats, including use of T cell lines and strictly in vitro approaches, have precluded significant advancement in this field (29–31). Other studies focused on the binding of LPC to receptors on the T cell surface but did not address whether specific molecules regulated transport of these phospholipid species across the cell membrane and into T cells (24, 32–34).

In this study, we investigated a role for MFSD2A in the effector CD8$^+$ T cell immune response. We showed that MFSD2A is required for transport of LPC into activated T cells. Loss of MFSD2A resulted in reduced memory T cell maintenance in vivo after primary *Listeria* infection. Mechanistically, MFSD2A-deficient cells were at a competitive disadvantage, unable to efficiently turnover at memory timepoints, which resulted in continued loss of these cells over time. Moreover, secondary response to infection was impaired in the absence of MFSD2A, most likely because of an overall decreased memory T cell pool. Thus, this study reveals a previously unknown process by which MFSD2A directs import of LPC species into effector CD8$^+$ T cells, a process that is essential for the maintenance and turnover of memory CD8$^+$ T cells.

Materials and Methods

Mice

Mice were bred and housed in specific pathogen-free conditions in accordance with the Institutional Animal Care and Use Committee of the University of Pittsburgh. MFSD2A$^{f/f}$ mice were a gift from D. Silver (Duke-NUS Medical School) and crossed to CD4cre$^+$ and Vα2-Vβ5 (OT-I) TCR transgenic mice (The Jackson Laboratory) to generate MFSD2A$^{f/f}$ CD4cre$^+$ OT-I$^+$ mice.

Competitive adoptive transfer experiments were performed by transferring a mixture of 1×10^4 wild-type (WT) CD45.1.2 OT-I$^+$ cells and 1×10^4 CD45.2 MFSD2A$^{f/f}$ CD4cre$^+$ OT-I$^+$ cells in a 1:1 ratio into CD45.1 recipient mice. MFSD2A$^{f/f}$ CD4cre$^+$ OT-I$^+$ mice were generated on a C57BL/6 background, and we determined no T cell rejection associated with minor MHC incompatibility.

Mixed bone marrow chimeras were generated by transferring a mixture of 2.5×10^6 B220$^-$CD3$^-$NK1.1$^-$ bone marrow cells from a CD45.1.2 WT donor and 2.5×10^6 B220$^-$CD3$^-$NK1.1$^-$ bone marrow cells from a CD45.2 MFSD2A$^{f/f}$ CD4cre$^+$ donor into lethally irradiated (1000 rad) CD45.1 recipient mice. All chimeras were rested at least 8 wk to allow reconstitution of the host.

For infectious studies, mice were infected i.v. the following day with 5000 CFU *Listeria*-OVA. *Listeria*-OVA was grown to late log-phase growth.

Flow cytometry

Single-cell suspensions were prepared from specified tissues. Cells were counted prior to staining. The following Abs were used: CD45.1–eFlour 450 (A20), CD45.1-BUV395 (A20; BD Biosciences) CD45.2-allophycocyanin (104), CD8–eFlour 506 (53-6.7), Vα2-PE (B20.1), CD44-PerCP-Cy5.5 (IM7), CD62L-allophycocyanin–eFluor 780 (MEL-14), KLRG1-PE–eFluor 610 (2F1), CD127-FITC (A7R34), H-2 kb OVA-tetramer PE (MBL International), IFN-γ–PE–eFluor 610 (XMG1.2), TNF-α–eFluor 450 (MP6-XT22), IL-2–PE-Cy7 (JES6-5H4), CD4-PE (GK1.5), CD1d–tetramer BV421 (National Institutes of Health Tetramer Core Facility), MFSD2A (provided by Dr. D. Silver), and TCRβ-allophycocyanin–eFluor 780 (H57-597). BrdU incorporation was detected by intracellular staining (APC BrdU Flow kit; BD Pharmingen). All Abs were purchased from Thermo Fisher Scientific (eBioscience) unless stated otherwise. Samples were fixed and permeabilized using CytoFix/CytoPerm Kit (BD Biosciences) or the Foxp3 staining kit (eBioscience) according to manufacturer's instructions. Samples were filtered and then collected on an LSR II, LSRFortessa, or FACSAria (BD Biosciences) and analyzed using FlowJo software (Tree Star).

In vitro assays

A total of 1×10^6 WT and MFSD2A-deficient CD8 T cells were stimulated in vitro with 2 μg/ml anti-CD28 (eBioscience) for the indicated amount of time in a 24-well dish precoated with 10 μg/ml anti-CD3 (eBioscience). Naive cells received 10 ng/ml IL-7 for maintenance. Cells were negatively selected for CD8$^+$ over columns (Miltenyi Biotec) prior to plating using biotinalyted Abs and streptavidin-conjugated microbeads (Miltenyi Biotec). For TopFluor-LPC assays (Avanti Polar Lipids), 0.1 μM TopFluor-LPC was added during the last 4 h of culture. CellTrace Violet assays were performed according to the manufacturer's protocol (eBioscience). All cell culture was performed in complete T cell media.

TLC

A total of 1×10^6 CD8$^+$ T cells were stimulated in vitro with anti-CD3 and anti-CD28 for 48 h and incubated with 150 μM TF-LPC as described. Live cells were sorted for quantification prior to Bligh and Dyer method of lipid extraction. Unloaded TopFluor-LPC was used as a control. Samples were loaded onto silica gel (EMD Millipore), and TF-LPC migration was visualized on a ProteinSimple FluorChem machine.

Quantitative PCR

A total of 1×10^6 WT or MFSD2A-deficient CD8 T cells were stimulated in vitro with anti-CD3 and anti-CD28 for the indicated amount of time. RNA was extracted from cell lysates using either the TRIzol (Ambion) method or RNeasy PLUS Micro Kit (QIAGEN). cDNA synthesis was performed using the All-in-One First-Strand cDNA synthesis kit, and quantitative PCR was performed using All-in-One SYBR Green (both GeneCopoeia) on a LightCycler 96 (Roche) using the following primers: MFSD2A forward, 5′-AGAAGCAGCAACTGTCCATTT-3′; and MFSD2A reverse, 5′-CTC GGCCCACAAAAAGGATAA T-3′. TaqMan probes (Thermo Fisher Scientific) were used for quantification of Srebp1.

Seahorse metabolic flux analyzer

Competitive adoptive transfer mice were generated and infected with *Listeria*-OVA as described above. Mice were taken out to day 40 postinfection (memory) prior to sorting for MFSD2A$^{+/+}$ and MFSD2A$^{-/-}$ OT-I CD8 T cells. Cells were plated in equal amounts on Seahorse Metabolic Flux Analyzer (Agilent Technologies) and analyzed using the XF Cell Mito Stress Test. A total of 200,000 cells were seeded into Cell-Tak–coated XFe96 plates in minimal unbuffered assay media containing 10 mM glucose, 1 mM sodium pyruvate, and 2 mM glutamine. Basal oxygen consumption and extracellular acidification rates (ECAR) were taken for 30 min. Cells received sequential injections of 2 μM oligomycin, 2 μM FCCP, 10 mM 2-deoxyglucose, and 0.5 μM rotenone/antimycin A.

Live cell imaging

MFSD2A$^{+/+}$ and MFSD2A$^{-/-}$ CD8$^+$ T cells were activated in vitro and cultured with TF-LPC as described above. Prior to imaging, cells were stained with Hoechst at a 1:1000 dilution at 4°C. Stain was rinsed twice

Downloaded from http://www.jimmunol.org/ by guest on February 24, 2022

with PBS prior to microscopy. Samples were imaged using a Nikon A1 point scanning confocal with a 60× 1.40 numerical aperture objective and Tokai Hit environmental controller. Complete volumes of cells were acquired at 1-μm steps, and volumes were reconstructed and analyzed using Nikon's NIS-Elements software. To define perinuclear space, a threshold was established using the nuclear signal labeled with Hoechst fluorescent nuclear marker. The nuclear threshold was then dilated, and the original nuclear threshold was subtracted from the dilated mask, leaving behind a region corresponding to the immediate perinuclear space in the cell, under which intensity measurements were performed.

Lipidomic analysis

The cell pellets were extracted using butanol-methanol. Briefly, 200 μl of the butanol-methanol (1/1; v/v) containing SPLASH internal standards solution were added to the samples. Samples were then sonicated for 30 min. One hundred ninety microliters of the lipid extracts were transferred into a new tubes, dried in a rotary evaporator, and resuspended with the same volume of mobile phase (hydrophilic interaction liquid chromatography [HILIC] mobile phase B: 95% acetonitrile + 5% aqueous 25 mM ammonium formate). Seventy microliters of lipid extracts were pooled from three biological replicates according to their genotype and activation state. From the pooled lipid extracts, 30 μl were used for PC analysis. The remaining 180 μl of the pooled lipid extracts was dried in a rotary evaporator, then resuspended in 60 μl of mobile phase (HILIC mobile phase B: 95% acetonitrile + 5% aqueous 25 mM ammonium formate, pH 4.6) prior to mass spectrometry analysis. The concentrated lipid extracts were used for the analysis of LPC, lysophosphatidylethanolamine (LPE), phosphatidylethanolamine (LEA), plasmalogen-PE-LEA, phosphatidylglycerol, phosphatidylinositol, and sphingomyelin. Samples were randomized for injection into a liquid chromatography–tandem mass spectrometry instrument (1290 Infinity II Liquid Chromatography System and 6490 QqQ, Agilent Technologies). Quality controls and blanks were injected after every five injections to monitor stability of the instrument response and carry-over. The chromatographic column was a Kinetex HILIC (150 × 2.1 mm, 2.6 μM, 100 Å; Phenomenex). Gradient elution was undertaken with solvents A (50% acetonitrile/50% aqueous 25 mM ammonium formate buffer, pH 4.6) and B (95% acetonitrile/5% aqueous 25 mM ammonium formate buffer, pH 4.6), with a gradient range from 99.9 to 75% solvent B in 6 min, 75–10% solvent B in 1 min, 10–99.9% solvent B in 0.1 min, and 10–99.9% solvent B for 3 min (total run time of 10.1 min). Phospholipids were quantified at the sum composition level, using multiple reaction monitoring with precursor to headgroup transitions. Phospholipids with fatty acid sum composition containing four double bonds were considered arachidonic acid containing, whereas phospholipids with a fatty acid sum composition containing six double bonds were considered DHA-containing. Mass spectrometry parameters were gas temperature of 200°C, gas flow of 12 l/min, sheath gas flow of 12 l/min, and capillary voltage of 3500 V. Quantification data were extracted using MassHunter Quantitative Analysis (QQQ) software, and data were manually curated to ensure correct peak integration. Areas under the curve for the extracted ion chromatograms for each multiple reaction monitoring transition and lipid species were normalized to internal standard and total cell counts. Isotope correction was then done on all relevant lipid species using an in-house R script.

Statistical analysis

All graphs were created using GraphPad Prism 7, and statistical significance was determined with the two-tailed unpaired Student *t* test or using one-way ANOVA adjusted for multiple comparisons where appropriate.

Results

LPC is actively transported into activated CD8$^+$ T cells

MFSD2A has previously been described as an essential transporter of LPC across the BBB (16). We first determined, using fluorescently labeled LPC (TopFluor-LPC), that CD8$^+$ T cells activated in vitro with anti-CD3 and anti-CD28 import TopFluor-LPC relative to naive T cells (Fig. 1A). To confirm this finding, we extracted lipids from naive or activated T cells that had been cultured with TopFluor-LPC and determined, using TLC, that only lipid extracts from activated T cells contained detectable levels of TopFluor-LPC (Fig. 1B). We next confirmed that import of TopFluor-LPC by activated T cells was not a function of either their size or passive uptake of TopFluor-LPC after proliferation. To address this, we labeled CD8$^+$ T cells with CellTrace Violet and, as before, activated these cells in vitro with anti-CD3 and anti-CD28. Notably, activated T cells that had not yet proliferated, as well as cells that had divided, imported more TopFluor-LPC relative to naive T cells (Fig. 1C). These data indicate that import of LPC into T cells is an activation dependent and active process.

MFSD2A is upregulated on activated CD8$^+$ T cells

Previous reports have indicated that LPC esterified to the LCFA DHA is transported across the BBB by the protein transporter MFSD2A. Because we observed that LPC is imported by activated T cells in vitro, we next determined the levels of MFSD2A expression on these activated T cells. MFSD2A mRNA and median fluorescence intensity (MFI) increased in CD8$^+$ T cells activated in vitro with anti-CD3 and anti-CD28, relative to naive cells (Fig. 1D, 1E). We therefore concluded that MFSD2A is upregulated on in vitro–activated CD8$^+$ T cells, potentially to actively transport LPC into these cells.

Conditional loss of MFSD2A does not affect T cell development but results in reduced LPC uptake by activated CD8$^+$ T cells

To establish the function of MFSD2A in activated CD8$^+$ T cells, we used a conditional deletion model system. We crossed MFSD2A floxed mice to mice expressing CD4-Cre recombinase (hereafter called MFSD2A$^{-/-}$ mice). After sorting CD8$^+$ T cells from the spleens of MFSD2A$^{+/+}$ and MFSD2A$^{-/-}$ mice and activating these cells in vitro for 72 h, we found that MFSD2A mRNA was reduced in the MFSD2A$^{-/-}$ T cells, indicating our Cre deletion system is robust (Fig. 2A, left). Additionally, comparison of MFSD2A expression levels by flow cytometry showed that MFSD2A$^{-/-}$ T cells expressed MFSD2A levels comparable with naive T cells (Fig. 2A, right). To confirm that MFSD2A expression was not required for thymocyte development, we examined T cell development in the thymus in the absence of MFSD2A. We did not observe any detectable differences in either CD4 and CD8 expression or total thymic cellularity or thymic subsets (Fig. 2B). Similarly, in peripheral lymphoid organs such as the spleen, total frequency of CD4, CD8, and invariant NKT cells was normal in the MFSD2A$^{-/-}$ animals relative to their WT counterparts (Fig. 2C). We did note a significant increase in the number of MFSD2A$^{-/-}$ cells in the spleen (Fig. 2C) but could not attribute this to increased T cell activation based on CD44, CD69, or CD25 expression (data not shown).

As we showed that activated CD8$^+$ T cells import TopFluor-LPC (Fig. 1), we next determined if this process was dependent on MFSD2A expression, as previously reported for endothelial cells at the BBB and retinal brain barrier (16, 17). We activated MFSD2A$^{+/+}$ and MFSD2A$^{-/-}$ CD8$^+$ T cells in vitro with anti-CD3 and anti-CD28 for 48 h, adding TopFluor-LPC during the last 4 h of culture. Import of TopFluor-LPC was significantly reduced in MFSD2A$^{-/-}$ CD8$^+$ T cells relative to MFSD2A$^{+/+}$ cells, although not to levels observed in naive T cells (Fig. 3A).

To further clarify whether MFSD2A expression was required to import LPC species into activated CD8$^+$ T cells, we compared global LPC and PC species in naive and 48 h in vitro–activated MFSD2A$^{+/+}$ and MFSD2A$^{-/-}$ CD8$^+$ T cells using mass spectrometry lipidomic analysis (Supplemental Fig. 1A, 1B). Activated MFSD2A$^{-/-}$ CD8$^+$ T cells trended toward lower detectable phospholipids, although there were some exceptions, including LPC 16:0 and LPC 18:0. Because of the overall low percentages of detectable endogenous phospholipid species, we used live cell imaging to determine uptake of exogenous LPC by MFSD2A in activated CD8$^+$ T cells. Here we discovered that TopFluor-LPC

Downloaded from http://www.jimmunol.org/ by guest on February 24, 2022

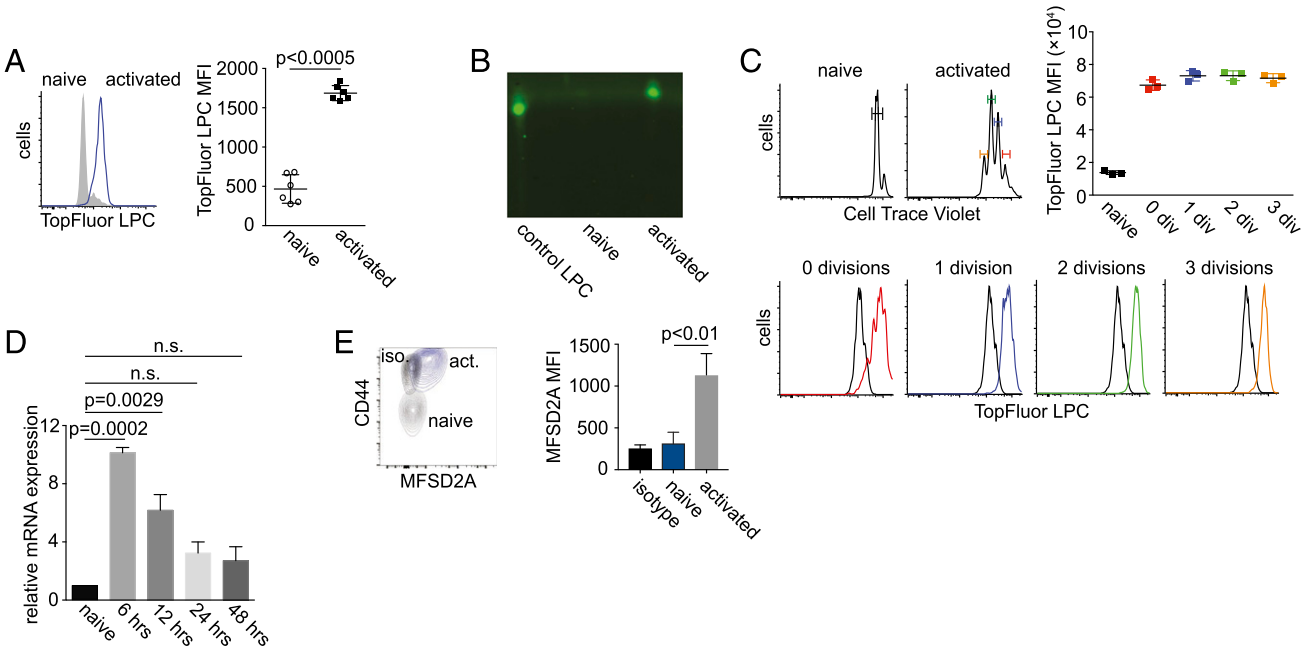

FIGURE 1. Activated CD8+ T cells import TopFluor-LPC and express MFSD2A. WT CD8+ T cells were activated in vitro with anti-CD3 and anti-CD28 for 72 h. TopFluor-LPC was added to naive or activated T cells for the last 4 h of culture. Naive cells were cultured with 10 ng/ml IL-7 for maintenance. (**A**) Histogram showing uptake of TopFluor-LPC by activated CD8+ T cells relative to naive cells. Graph shows MFI of TopFluor-LPC in activated versus naive T cells. (**B**) TLC of lipids extracted from cells described in (A). TopFluor-LPC alone was used as a loading control. (**C**) Histograms showing CellTrace Violet dilution by naive and activated CD8+ T cells stimulated as in (A). Graph and lower histograms indicate the TopFluor-LPC imported by these cells based on the number of divisions as identified by CellTrace Violet dilution. (**D**) Relative mRNA expression of *Mfsd2a* in CD8+ T cells activated with anti-CD3 and anti-CD28 in vitro for the indicated time period. Data were normalized to Mfsd2a expression in naive T cells. (**E**) Flow cytometry plot and bar graph showing MFSD2A expression in gated CD8+ T cells activated for 72 h in vitro. Expression of CD44 is shown for comparison. Iso (black) indicates isotype control. Error bars show average and SEM. The *p* values were calculated using one-way ANOVA. Data are representative of three independent experiments (A–C) or two independent experiments (D and E) with one to three mice per experiment.

localized at the perinuclear space in activated MFSD2A$^{+/+}$ CD8+ T cells relative to either activated MFSD2A$^{-/-}$ cells or naive cells (Fig. 3B). As the perinuclear space is continuous with the smooth endoplasmic reticulum, a site of phospholipid synthesis, fatty acid elongation, and fatty acid desaturation (35), we postulate that LPC species are being used by activated CD8+ T cells in these processes. Together, our data indicate that MFSD2A expression is dispensable for T cell development but that it is required for import of LPC after T cell activation. We also show that imported LPC localizes at the perinuclear space in activated CD8+ T cells.

The primary immune response to infection by MFSD2A-deficient CD8+ T cells is unimpaired

We next examined MFSD2A$^{-/-}$ CD8+ T cells over the course of an intracellular bacterial infection. We generated MFSD2A$^{-/-}$ OT-I TCR transgenic T cells (CD45.2) that recognize OVA peptide, which were adoptively cotransferred with MFSD2A$^{+/+}$ OT-I T cells (CD45.1.2) into naive recipients and distinguished from host cells (CD45.1) by congenic CD45 expression. Recipient mice were infected i.v. with *Listeria monocytogenes* expressing OVA (*Listeria*-OVA), and the immune response in the blood was monitored postinfection. We observed no difference in the MFSD2A$^{-/-}$ OT-I cell response during the primary infection (Fig. 4A, 4B). When we measured the number of OT-I T cells in the spleens of infected mice, we detected a slight decrease in MFSD2A$^{-/-}$ OT-I cells at day 7 postinfection that we could not detect at day 10 postinfection (Supplemental Fig. 2A).

To further characterize MFSD2A$^{-/-}$ CD8+ T cells during the primary immune response, we harvested spleens of recipient mice and analyzed MFSD2A$^{+/+}$ and MFSD2A$^{-/-}$ OT-I cells during infection. We detected a decrease in the frequency of KLRG1^{lo} CD127^{hi} memory precursor cells in MFSD2A$^{-/-}$ OT-I cells in the PBL and in the spleen on days 7 and 10 postinfection (Supplemental Fig. 2B). When we examined intracellular cytokine expression by MFSD2A$^{+/+}$ and MFSD2A$^{-/-}$ cells after restimulation in vitro with OVA, we determined that MFSD2A deficiency resulted in a small but significant reduction in IFN-γ+ TNF-α+–expressing cells at day 10 postinfection (Fig. 4C). We thus concluded loss of MFSD2A expression on CD8+ T cells resulted in decreased cytokine production and reduced frequency of KLRG1^{lo} CD127^{hi} memory precursors during the primary T cell immune response.

To determine the endogenous CD8+ T cell response to *Listeria*-OVA in a competitive environment, we generated mixed bone marrow chimeras with a 1:1 mix of MFSD2A$^{+/+}$ (CD45.1.2) and MFSD2A$^{-/-}$ (CD45.2) bone marrow and infected the recipient mice 8 wk after reconstitution. Upon infection with *Listeria*-OVA, we determined the frequency of MFSD2A$^{+/+}$ and MFSD2A$^{-/-}$ OVA-tetramer+ T cells throughout the course of the infection. As with the adoptive transfer of OT-I T cells, we observed little difference in the frequency of MFSD2A$^{+/+}$ and MFSD2A$^{-/-}$ tetramer+ CD8+ T cells in the PBL over time (Supplemental Fig. 3A, 3B). However, as before, MFSD2A$^{-/-}$ cells were defective in IFN-γ production postinfection (Supplemental Fig. 3C). Overall, we found that loss of MFSD2A expression on CD8+ T cells resulted in modestly decreased cytokine production by these cells during primary infection.

Impaired memory T cell maintenance by MFSD2A-deficient CD8+ T cells in a competitive environment

Although we detected no significant difference in frequency between MFSD2A$^{+/+}$ and MFSD2A$^{-/-}$ cells at early memory timepoints

Downloaded from http://www.jimmunol.org/ by guest on February 24, 2022

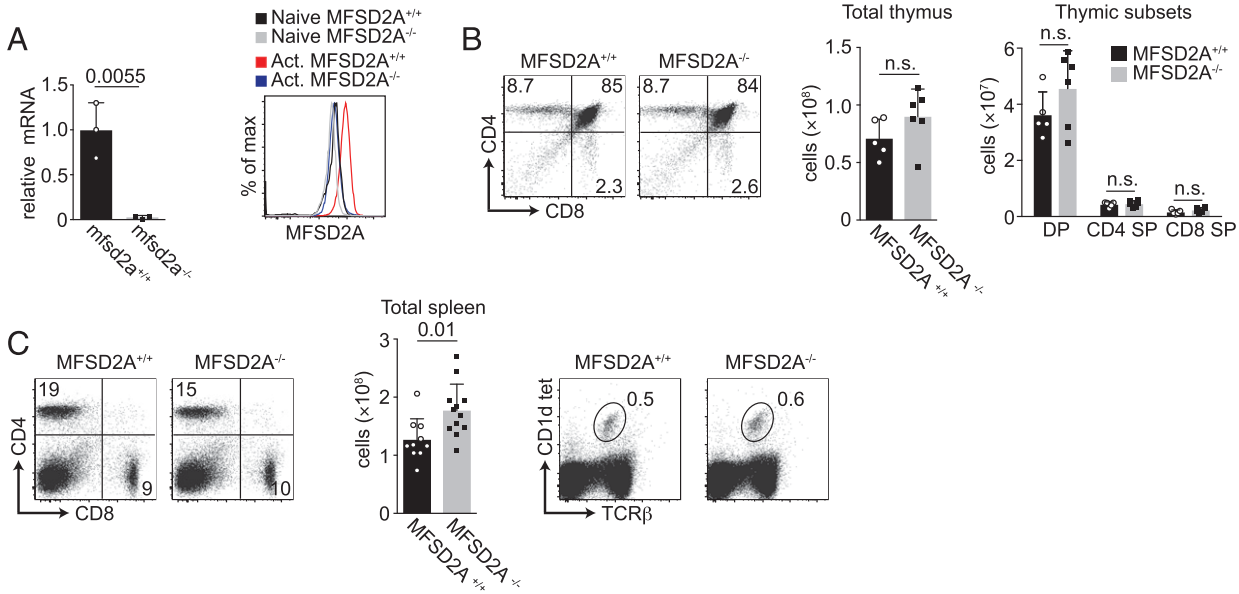

FIGURE 2. Thymic development in conditional MFSD2A mice is normal. (**A**) Graph indicates relative mRNA expression of Mfsd2a in 72 h in vitro–activated CD8$^+$ T cells from WT (Mfsd2a$^{+/+}$) and Mfsd2a floxed mice crossed to CD4-Cre (Mfsd2a$^{-/-}$). Histogram indicates MFSD2A expression by naive and 72 h in vitro–activated CD8$^+$ T cells from the indicated genotype. (**B**) Flow cytometry plots indicating CD4 and CD8 expression in thymocytes from MFSD2A$^{+/+}$ and MFSD2A$^{-/-}$ mice. Graphs indicate total cells and the proportion of double positive (DP), CD4 single positive (SP), and CD8 SP total T cells from the thymus of MFSD2A$^{+/+}$ and MFSD2A$^{-/-}$ mice. (**C**) Flow cytometry plots (left) indicating CD4 and CD8 expression on T cells from the spleens of MFSD2A$^{+/+}$ and MFSD2A$^{-/-}$ mice. Graph indicates total splenocyte number from MFSD2A$^{+/+}$ and MFSD2A$^{-/-}$ mice. Flow cytometry plots (right) indicate TCRβ and CD1d tetramer staining on invariant NKT cells from the spleen of MFSD2A$^{+/+}$ and MFSD2A$^{-/-}$ mice. Numbers indicate the frequency of cells within the gate. Data are representative of two to three independent experiments with each dot indicating an individual mouse. Error bars show average and SEM. The *p* values were calculated using the Student *t* test or using one-way ANOVA adjusted for multiple comparisons.

postinfection (Fig. 4B), by day 40 postinfection we observed a reduction in the frequency of MFSD2A-deficient OT-I cells in the PBL and spleen (Fig. 5A). At this memory timepoint, we also observed that fewer MFSD2A-deficient cells were KLRG1^{lo}CD127^{hi} and CD44^{hi}CD62L^{hi} relative to their WT counterparts (Fig. 5B), suggesting that the remaining MFSD2A-deficient cells were likely terminally differentiated effector cells. Restimulation with OVA revealed that these cells were also deficient in production of IFN-γ$^+$ and TNF-α$^+$ at day 40 postinfection (Fig. 5B). To determine that the loss of MFSD2A-deficient cells was not due to inability of these memory cells to home to the lymphoid organs, we examined CCR7 expression on splenic MFSD2A$^{+/+}$ and MFSD2A$^{-/-}$ cells and did not observe a difference in CCR7 expression (data not shown). Additionally, we evaluated TopFluor-LPC uptake after 6 h stimulation in vitro in the MFSD2A-deficient cells at day 40 postinfection. We confirmed TopFluor-LPC uptake was minimally reduced in the absence of MFSD2A (Fig. 5C), indicating that memory MFSD2A$^{-/-}$ cells had reduced ability to import LPC upon restimulation.

Recent data have shown that the SREBPs, which are proteins required for lipogenesis and subsequent membrane synthesis, are upregulated in the brain to compensate for loss of MFSD2A and LPC import (21). Thus, we decided to investigate if loss of MFSD2A in CD8$^+$ T cells would also result in upregulation of the Srebp genes. We observed that in vitro restimulated CD8$^+$ MFSD2A$^{-/-}$ memory T cells showed increased mRNA expression levels of the gene *Srebp1*, indicating that de novo lipogenesis pathways may be increased in the absence of MFSD2A in activated memory CD8$^+$ T cells (Fig. 5D). We next determined the rates of glycolysis and

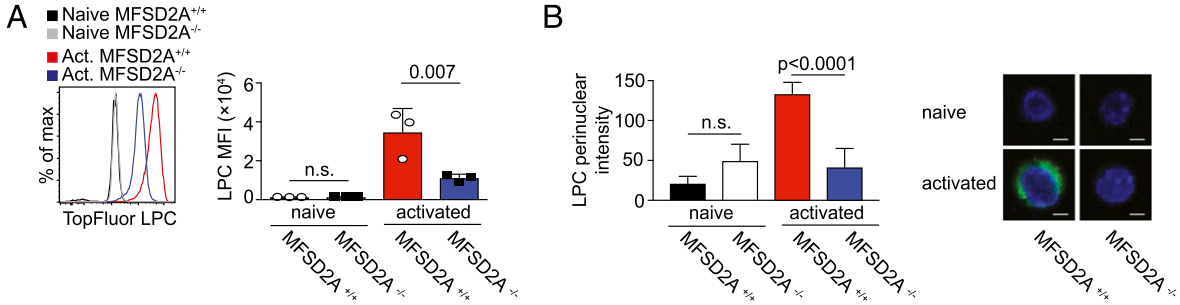

FIGURE 3. LPC uptake is reduced in MFSD2A-deficient activated CD8$^+$ T cells. (**A**) Histogram showing uptake of TopFluor-LPC by MFSD2A$^{+/+}$ and MFSD2A$^{-/-}$ CD8$^+$ T cells stimulated with anti-CD3 and anti-CD28 for 48 h in vitro. TopFluor-LPC was added during the last 4 h of culture. Naive MFSD2A$^{+/+}$ and MFSD2A$^{-/-}$ CD8$^+$ T cells cultured with TopFluor-LPC for 4 h are shown for comparison. Graph indicates the MFI of TopFluor-LPC in MFSD2A$^{+/+}$ and MFSD2A$^{-/-}$ cells. (**B**) Live cell imaging of naive or activated (48 h with anti-CD3 and anti-CD28) MFSD2A$^{+/+}$ and MFSD2A$^{-/-}$ CD8$^+$ T cells cultured for the final 4 h with TopFluor-LPC. Graph indicates the TopFluor-LPC localized within the perinuclear mask. Images indicate representative cells with Hoechst staining for comparison. Scale bar, 2.5 μm. Data in (A) are representative of two independent experiments, with each dot indicating an individual mouse. Data in (B) are representative of five individual cells per condition and genotype imaged after culture with TopFluor-LPC. Error bars show average and SEM. The *p* values were calculated using the Student *t* test or using one-way ANOVA adjusted for multiple comparisons.

Downloaded from http://www.jimmunol.org/ by guest on February 24, 2022

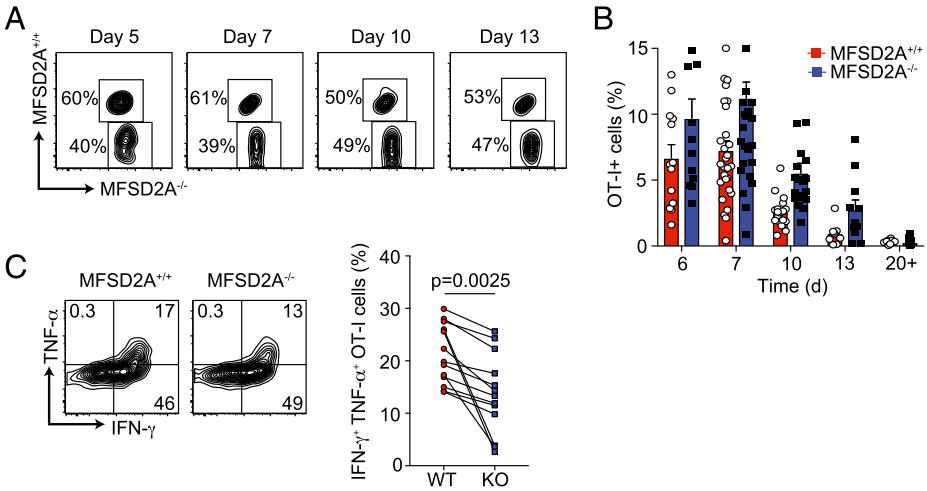

FIGURE 4. CD8$^+$ effector T cell frequency and function in the absence of MFSD2A. (**A**) Flow cytometry plots showing the frequency of gated OT-I$^+$ CD8$^+$ adoptively transferred MFSD2A$^{+/+}$ (CD45.1.2) and MFSD2A$^{-/-}$ (CD45.2) cells in the PBL on the indicated days postinfection with *Listeria*-OVA. (**B**) Graph indicating the frequency of MFSD2A$^{+/+}$ and MFSD2A$^{-/-}$ OT-I$^+$ T cells in the PBL (as a percentage of total live lymphocytes) on the indicated day postinfection. Each dot represents one individual mouse. (**C**) Flow cytometry plots showing intracellular staining for TNF-α and IFN-γ in MFSD2A$^{+/+}$ and MFSD2A$^{-/-}$ OT-I T cells isolated from the spleen on day 10 postinfection. Cells were restimulated in vitro with OVA peptide for 6 h before intracellular staining. Graph indicates the frequency of IFN-γ$^+$ TNF-α$^+$ OT-I MFSD2A$^{+/+}$ and MFSD2A$^{-/-}$ cells on day 10 postinfection. Each dot pair indicates data from one host animal. Data are representative of three to six independent experiments with two to five mice per timepoint per experiment. Error bars show average and SEM. The *p* values were calculated using the paired Student *t* test.

mitochondrial respiration in memory MFSD2A$^{+/+}$ and MFSD2A$^{-/-}$ OT-I T cells using the Seahorse Extracellular Flux Analyzer. We consistently observed slightly increased higher oxygen consumption rates (OCR) and ECAR as well as increased spare respiratory capacity (SRC) (Fig. 5E). We propose that loss of LPC and LCFAs in MFSD2A$^{-/-}$ cells forces these cells to increase their metabolic activity upon restimulation, possibly because of increased de novo lipogenesis, to compensate for loss of LPCs and LCFAs.

Impaired T cell response to secondary infection by MFSD2A-deficient CD8$^+$ T cells in a competitive environment

We determined *mfsd2a* mRNA expression in MFSD2A$^{+/+}$ cells at memory (day 40) after primary infection and at day 2.5 after secondary infection with high-dose *Listeria*-OVA (1×10^5 CFU) (Fig. 6A). Similar to its expression after primary infection, *mfsd2a* mRNA was upregulated on OT-I CD8$^+$ T cells after secondary infection (Fig. 6A). To determine the secondary immune response in the absence of MFSD2A, we reinfected mice at day 40 postinfection with high-dose *Listeria*-OVA (1×10^5 CFU). Although MFSD2A$^{+/+}$ cells responded with normal kinetics, reinfection resulted in a severely impaired secondary response by the MFSD2A$^{-/-}$ cells (Fig. 6B). By day 5 after secondary infection, we could detect ~3% OT-I$^+$ MFSD2A$^{-/-}$ cells in the spleen relative to 96% MFSD2A$^{+/+}$ cells (Fig. 6C). We concluded that restimulation of MFSD2A$^{-/-}$ cells resulted in reduced secondary response to infection, owing to poor memory T cell differentiation and formation.

Importantly, we observed a similar deficiency in the endogenous memory and secondary response in our 1:1 mixed bone marrow chimeras (Supplemental Fig. 4A, 4B). At day 40 postinfection, we determined that there was a substantial reduction in the frequency of OVA-tetramer$^+$ CD45.2$^+$ MFSD2A$^{-/-}$ cells relative to MFSD2A$^{+/+}$ cells and that upon secondary infection with *Listeria*-OVA, these MFSD2A$^{-/-}$ cells did not respond as robustly as MFSD2A$^{+/+}$ cells (Supplemental Fig. 4A, 4B). IFN-γ production was also decreased in splenic MFSD2A$^{-/-}$ cells at day 6 after secondary infection. To confirm these data using a different infection model, we also infected mixed bone marrow chimeras with *Listeria*-gp33 and similarly showed a reduction in gp33-tetramer$^+$ cells at memory (data not shown). We also examined how endogenous MFSD2A$^{-/-}$ cells responded to primary and secondary infection in a noncompetitive environment. Here we directly infected either MFSD2A$^{+/+}$ or MFSD2A$^{-/-}$ mice and observed the endogenous response to *Listeria*-OVA. Interestingly, when MFSD2A$^{-/-}$ cells were not forced to compete with MFSD2A$^{+/+}$ cells, their response during the primary infection and at memory timepoints was comparable with that of MFSD2A$^{+/+}$ cells (Supplemental Fig. 4C). During their secondary response to infection, we observed a reduction in the MFSD2A$^{-/-}$ cells at days 5 and 7 postinfection, although the difference was NS (Supplemental Fig. 4D). These data indicate that MFSD2A deficiency affects CD8$^+$ T cell memory formation and secondary response only when the MFSD2A-sufficient and -deficient cells are required to compete for resources, such as LPC phospholipid species.

To determine specifically why MFSD2A deficiency resulted in poor memory T cell maintenance and secondary immune response, we assessed the proliferative capacity of OT-I memory T cells. BrdU incorporation from days 25–40 postinfection demonstrated that MFSD2A$^{-/-}$ cells were dividing significantly less than MFSD2A$^{+/+}$ cells (Fig. 6D). Additionally, analysis of Ki-67 expression confirmed that ~5% MFSD2A$^{-/-}$ memory cells were in active cell cycle relative to ~15% of the MFSD2A$^{+/+}$ memory cells (Fig. 6E). We determined that loss of MFSD2A expression during the early T cell effector phase deprived CD8$^+$ T cells of LPC and LCFAs, resulting in reduced proliferation and turnover of these cells. We concluded that loss of MFSD2A expression negatively affected the ability of memory T cells to undergo homeostatic proliferation at memory timepoints.

As we observed a decrease in in the frequency of KLRG1^{lo} CD127^{hi} memory precursor cells in MFSD2A$^{-/-}$ OT-I cells (Supplemental Fig. 2B), we were curious if the reduced proliferative capacity of OT-I memory T cells was due to the abundance of KLRG1^{hi} versus KLRG1^{lo} memory cells in the MFSD2A$^{+/+}$ versus MFSD2A$^{-/-}$ populations. To test this, we gated on KLRG1^{hi} versus KLRG1^{lo} MFSD2A$^{+/+}$ or MFSD2A$^{-/-}$ memory OT-I cells and assessed Ki-67 expression. We detected no difference in the homeostatic turnover of KLRG1^{hi} versus KLRG1^{lo} MFSD2A-sufficent cells (Fig. 6F). Both KLRG1^{hi} versus KLRG1^{lo}

Downloaded from http://www.jimmunol.org/ by guest on February 24, 2022

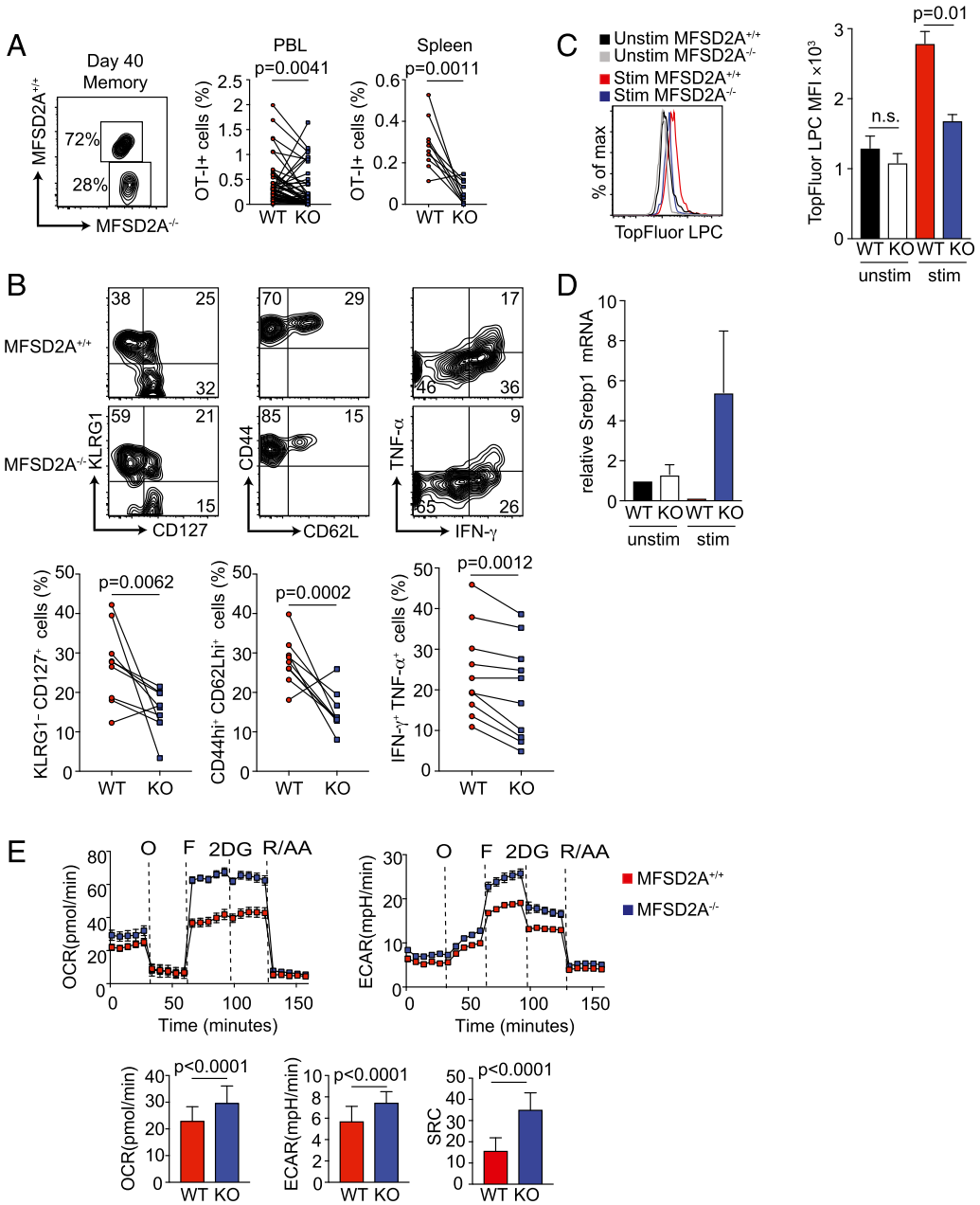

FIGURE 5. CD8$^+$ memory T cell frequency and function in the absence of MFSD2A. (**A**) Flow cytometry plot showing the frequency of OT-I$^+$ CD8$^+$ adoptively transferred MFSD2A$^{+/+}$ (CD45.1.2) and MFSD2A$^{-/-}$ (CD45.2) cells in the PBL at day 40 (memory) postinfection with *Listeria*-OVA. Graphs indicate the frequency of MFSD2A$^{+/+}$ (CD45.1.2) and MFSD2A$^{-/-}$ (CD45.2) OT-I T cells as a percentage of total live lymphocytes in the PBL or spleen. Each dot pair indicates data from one host animal. (**B**) Flow cytometry plots and graphs showing CD127, KLRG1, CD62L, CD44, IFN-γ, and TNF-α expression by gated OT-I MFSD2A$^{+/+}$ and MFSD2A$^{-/-}$ cells isolated from the spleen on day 45 postinfection. Cytokine expression was determined after stimulation in vitro for 6 h with OVA. Each dot pair indicates data from one host animal. (**C**) Histogram and bar graph indicating TopFluor-LPC MFI by OT-I MFSD2A$^{+/+}$ and MFSD2A$^{-/-}$ cells isolated from the spleen on day 45 postinfection and stimulated in vitro for 6 h with OVA and TopFluor-LPC. Cells that were isolated at day 45 and cultured with TopFluor-LPC but without OVA (unstim) are shown for comparison. (**D**) Graph indicating Srebp1 mRNA expression in memory or 48 h in vitro–activated memory MFSD2A$^{+/+}$ and MFSD2A$^{-/-}$ CD8$^+$ T cells. Data were normalized to unactivated memory MFSD2A$^{+/+}$ cells. (**E**) OCR trace, ECAR trace, and graphs showing basal OCR, ECAR, and SRC from OT-I MFSD2A$^{+/+}$ and MFSD2A$^{-/-}$ cells isolated from the spleen on day 45 postinfection, where "O" is oligomycin, "F" is FCCP, "2DG" is 2-deoxy-glucose, and "R/AA" is rotenone and antimycin A. SRC is calculated as the difference between initial OCR values and the maximal OCR values achieved after FCCP uncoupling. Data are representative of three to six independent experiments with two to five mice per timepoint per experiment (A–C), two independent experiments with two to three mice per group (D), or two independent experiments with two to three mice per experiment (E). Error bars show average and SEM. The *p* values were calculated using the Student *t* test or using one-way ANOVA adjusted for multiple comparisons.

MFSD2A-deficient cells showed reduced Ki-67$^+$ expression (Fig. 6F). Additionally, TopFluor-LPC uptake was decreased in memory MFSD2A$^{-/-}$ cells irrespective of KLRG1 expression (Fig. 6G). We concluded that memory T cell turnover and TopFluor-LPC uptake is reduced in the absence of MFSD2A, an effect that is not dependent on KLRG1 expression.

Discussion

In this article, we present evidence that the LPC transporter MFSD2A is required to maintain CD8$^+$ T cell memory. We showed that activated T cells can import LPC species and that expression of MFSD2A was required to support this process. Although the effect was subtle during the effector phase, loss of

Downloaded from http://www.jimmunol.org/ by guest on February 24, 2022

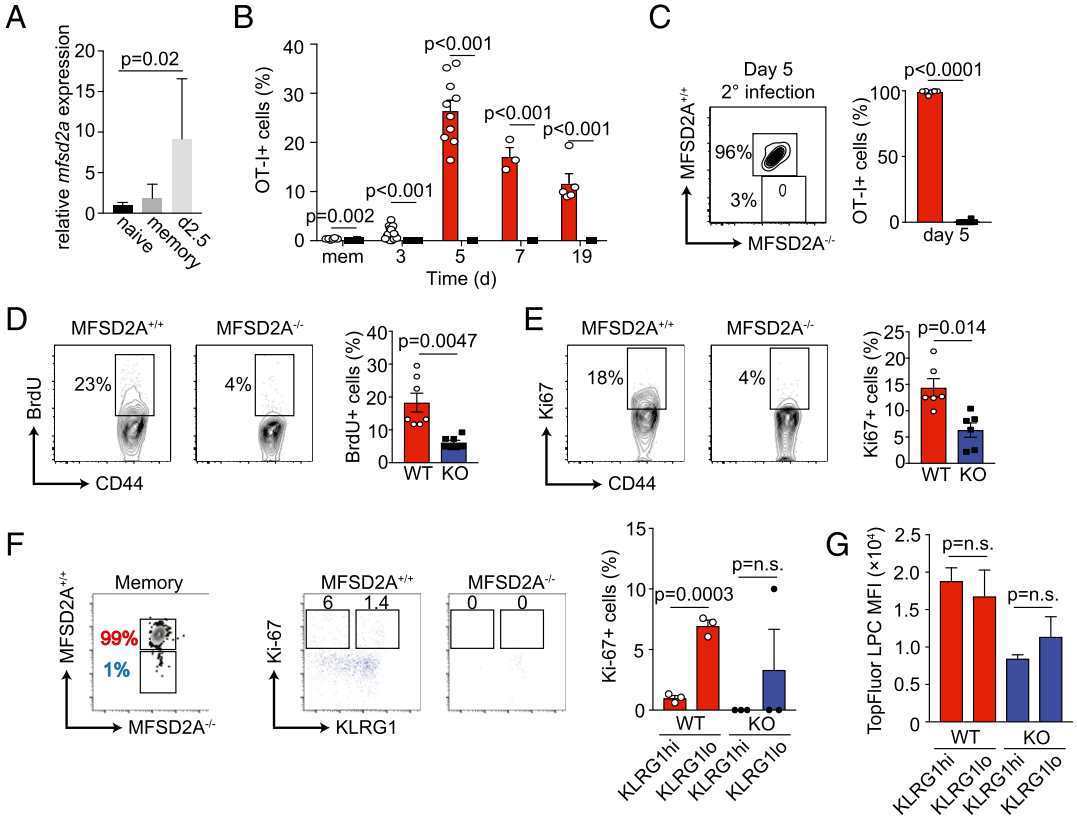

FIGURE 6. MFSD2A deficiency affects CD8+ T cell response to secondary infection. (**A**) Bar graph indicates relative mRNA expression of *Mfsd2a* in OT-I CD8+ T cells isolated at memory (day 40) or after secondary infection with *Listeria*-OVA (day 2.5 after secondary infection). Data were normalized to Mfsd2a expression in naive T cells. (**B**) Graph indicating the frequency of MFSD2A$^{+/+}$ and MFSD2A$^{-/-}$ OT-I^{+} T cells in the PBL on the indicated day after secondary infection with *Listeria*-OVA. Dots on graphs indicate individual mice. (**C**) Flow cytometry and bar graph showing the frequency of splenic OT-I MFSD2A$^{+/+}$ and MFSD2A$^{-/-}$ cells at day 5 (peak) after secondary infection with *Listeria*-OVA. (**D**) Flow cytometry and graph showing BrdU incorporation by cotransferred OT-I MFSD2A$^{+/+}$ and MFSD2A$^{-/-}$ cells isolated from the spleen on day 45 postinfection. BrdU (1 mg/ml) was added to the drinking water from day 25–40 postinfection. Dots on graphs indicate individual mice. (**E**) Flow cytometry and graph showing Ki-67 expression in cotransferred OT-I MFSD2A$^{+/+}$ and MFSD2A$^{-/-}$ cells isolated from the spleen on day 45 postinfection. (**F**) Flow cytometry and graphs showing Ki-67 expression on gated KLRG1^{hi} or KLRG1^{lo} cotransferred OT-I MFSD2A$^{+/+}$ and MFSD2A$^{-/-}$ cells isolated from the spleen on or after day 45 postinfection. (**G**) Bar graph indicating TopFluor-LPC MFI by gated KLRG1^{hi} or KLRG1^{lo} OT-I MFSD2A$^{+/+}$ and MFSD2A$^{-/-}$ cells isolated from the spleen on or after day 45 postinfection and stimulated in vitro for 6 h with OVA and TopFluor-LPC. Dots on graphs indicate individual mice. Data are representative of three independent experiments (A–C) or two independent experiments (D and E) with ≥3 mice per timepoint per experiment. Data in (F) and (G) are from three individual mice. Error bars show average and SEM. The *p* values were calculated using the Student *t* test or using one-way ANOVA adjusted for multiple comparisons.

MFSD2A expression on CD8+ effector T cells resulted in decreased IFN-γ and TNF-α production. At established memory timepoints (>40 d), the frequency of MFSD2A-deficient T cells was substantially reduced relative to their WT counterparts. This "failure to thrive" was a result of reduced homeostatic turnover at memory timepoints, a process that was independent of KLRG1 expression. Thus, subsequent secondary infection resulted in a severely muted T cell response in the MFSD2A-deficient T cells. Direct infection of MFSD2A$^{-/-}$ mice did not result in the same loss of memory T cells, as we observed with competitive adoptive cotransfer or with 1:1 mixed bone marrow chimeras. We concluded that loss of MFSD2A-deficient T cells at memory timepoints was dependent on a competitive inflammatory environment.

Why would early expression of a lipid transporter such as MFSD2A affect memory T cell maintenance? The answer may be found in our current understanding of memory T cell metabolism. A number of studies have determined that memory T cells rely primarily on OXPHOS to meet their energy requirements (36, 37). In memory CD8+ T cells, this process is fueled by cell-intrinsic lipolysis of endogenous fatty acids to produce glycerol and free fatty acids (4). Effector T cells, in contrast, are adept at import of exogenous fatty acids (4). Recent new data, however, have shown that although memory T cells can use OXPHOS, fatty acid oxidation is not essential for effector or memory T cell formation (14). In light of these new data, it is possible that LPC species coupled to LCFAs are used by effector and memory T cells for fatty acid synthesis and/or for biomembrane formation. A recent publication has shown that lipogenesis and Srebp activity is increased in the brain in the absence of MFSD2A, presumably to compensate for loss of LPCs (21), and our data indicate that the master transcriptional regulator of lipogenic gene expression Srebp1 mRNA is increased in MFSD2A-deficient activated memory CD8+ T cells. An increase in fatty acid synthesis with loss of MFSD2A might also explain why we see an increase in certain fatty acid species in in vitro–activated CD8+ T cells, including LPC 16:0 and LPC 18:0, in the absence of MFSD2A. Thus, loss of MFSD2A expression marginally affects the primary immune response but has a substantial effect on the differentiation of memory T cells. This potential mechanism is supported by recent published work in which inhibition of fatty acid synthesis during CD4+ T cell priming resulted in no effect on the primary effector response but did result in decreased memory T cell survival (38).

Downloaded from http://www.jimmunol.org/ by guest on February 24, 2022

Our results are in line with other work describing the import of exogenous metabolites to support either effector or memory T cells proliferation. AQP9 was shown to be essential for transport of glycerol into memory T cells, where it can be used for triacylglyceride synthesis to support long-term memory turnover (5). It is likely that this process continues in the absence of MFSD2A, but we propose that import of glycerol by AQP9 is unable to "keep up" with the lipogenesis demands of MFSD2A-deficient memory T cells, which were deprived of exogenous fatty acids during the effector phase. We also observed that MFSD2A-deficient memory T cells are more metabolically active. We postulate that this may be a compensatory mechanism for loss of LPC species during the effector phase. Similarly, the transporter GLUT1 is known to be critical for the transport of glucose into effector T cells (6, 27), to supply glucose for glycolysis during the effector response. In the absence of MFSD2A, we have observed reduced GLUT1 expression on effector $CD8^+$ T cells (data not shown), and MFSD2A and GLUT1 were reported to colocalize at the BBB (16, 19, 39). As the secondary metabolites of glycolysis have been reported to be essential for cytokine production by $CD4^+$ and $CD8^+$ effector T cells (6, 40), it is possible that loss of these secondary metabolites is responsible for the decreased cytokine production we observe in the absence of MFSD2A. Finally, exogenous large neutral amino acids are transported into effector T cells through the transporter Slc7a5, a process that is essential for their differentiation (7). Slc7a5-deficient cells fail to upregulate c-Myc, impairing their ability to upregulate their metabolic output in response to infection is impaired (7). There is no known link between MFSD2A and Slc7a5 expression, and it is likely these transporters can act independently of one another.

In plasma, LPC is most commonly esterified to stearate, oleate, palmitate, and DHA, although both oleate and palmitate LPCs are transported by MFSD2A at lower affinities than LPC-DHA (16). Our mass spectrometry data revealed a subtle reduction in LPC and PC species in the absence of MFSD2A in in vitro–activated primary $CD8^+$ T cells. Using TopFluor-LPC, which was previously shown to be transported by MFSD2A (16), we showed that LPC transport was reduced in the absence of MFSD2A and that fluorescently labeled LPCs could be detected by confocal microscopy at the perinucleus of WT activated cells but not MFSD2A-deficient cells. Thus, LPCs are transported into effector T cells through an MFSD2A-dependent mechanism. In the future, determining specifically how LPC is metabolized after transport into activated T cells will provide key insights into how LPC and LCFAs are used by $CD8^+$ T cells for membrane biosynthesis or in the modulation of gene expression.

Although mutations in MFSD2A in humans are extremely rare, several families with full or partial mutations in MFSD2A have been identified (18–20). Inactivating mutations resulted in microcephaly syndrome and increased LPC lipids in the plasma, presumably because of inadequate uptake at the BBB (19, 20). Similarly, partial inactivation of MFSD2A also affected brain development, resulting in patients with progressive microcephaly syndrome (18). Although the effector and memory T cell populations in the blood of these patients was not examined, it is interesting to speculate that these patients may have impaired or reduced memory $CD8^+$ T cell populations, perhaps resulting in reduced ability to fight repeat infection.

Overall, we show in this article that expression of the protein MFSD2A early during the $CD8^+$ effector T cell immune response has critical long-term effects on memory T cell formation and turnover. We propose that import of LCFAs coupled to LPC is critical to maintain the lipogenesis requirements of $CD8^+$ memory T cells, which when perturbed result in decreased response to secondary infection.

Acknowledgments

We would like to acknowledge Drs. Lawrence Kane, Sarah Gaffen, and Mandy McGeachy for critical reading of the manuscript and members of the D'Cruz laboratory for their constructive criticism and comments. We would also like to thank the University of Pittsburgh Unified Flow Core for assistance with cell sorting and flow cytometry.

Disclosures

The authors have no financial conflicts of interest.

References

1. Chang, J. T., E. J. Wherry, and A. W. Goldrath. 2014. Molecular regulation of effector and memory T cell differentiation. *Nat. Immunol.* 15: 1104–1115.
2. Buck, M. D., D. O'Sullivan, and E. L. Pearce. 2015. T cell metabolism drives immunity. *J. Exp. Med.* 212: 1345–1360.
3. Delgoffe, G. M., and J. D. Powell. 2015. Sugar, fat, and protein: new insights into what T cells crave. *Curr. Opin. Immunol.* 33: 49–54.
4. O'Sullivan, D., G. J. van der Windt, S. C. Huang, J. D. Curtis, C. H. Chang, M. D. Buck, J. Qiu, A. M. Smith, W. Y. Lam, L. M. DiPlato, et al. 2014. Memory CD8(+) T cells use cell-intrinsic lipolysis to support the metabolic programming necessary for development. [Published erratum appears in 2018 *Immunity* 49: 375–376.] *Immunity* 41: 75–88.
5. Cui, G., M. M. Staron, S. M. Gray, P. C. Ho, R. A. Amezquita, J. Wu, and S. M. Kaech. 2015. IL-7-Induced glycerol transport and TAG synthesis promotes memory CD8+ T cell longevity. *Cell* 161: 750–761.
6. Macintyre, A. N., V. A. Gerriets, A. G. Nichols, R. D. Michalek, M. C. Rudolph, D. Deoliveira, S. M. Anderson, E. D. Abel, B. J. Chen, L. P. Hale, and J. C. Rathmell. 2014. The glucose transporter Glut1 is selectively essential for CD4 T cell activation and effector function. *Cell Metab.* 20: 61–72.
7. Sinclair, L. V., J. Rolf, E. Emslie, Y. B. Shi, P. M. Taylor, and D. A. Cantrell. 2013. Control of amino-acid transport by antigen receptors coordinates the metabolic reprogramming essential for T cell differentiation. [Published erratum appears in 2014 *Nat. Immunol.* 15: 109.] *Nat. Immunol.* 14: 500–508.
8. Kidani, Y., H. Elsaesser, M. B. Hock, L. Vergnes, K. J. Williams, J. P. Argus, B. N. Marbois, E. Komisopoulou, E. B. Wilson, T. F. Osborne, et al. 2013. Sterol regulatory element-binding proteins are essential for the metabolic programming of effector T cells and adaptive immunity. *Nat. Immunol.* 14: 489–499.
9. Lochner, M., L. Berod, and T. Sparwasser. 2015. Fatty acid metabolism in the regulation of T cell function. *Trends Immunol.* 36: 81–91.
10. Michalek, R. D., V. A. Gerriets, S. R. Jacobs, A. N. Macintyre, N. J. MacIver, E. F. Mason, S. A. Sullivan, A. G. Nichols, and J. C. Rathmell. 2011. Cutting edge: distinct glycolytic and lipid oxidative metabolic programs are essential for effector and regulatory CD4+ T cell subsets. *J. Immunol.* 186: 3299–3303.
11. Pearce, E. L., M. C. Walsh, P. J. Cejas, G. M. Harms, H. Shen, L. S. Wang, R. G. Jones, and Y. Choi. 2009. Enhancing CD8 T-cell memory by modulating fatty acid metabolism. *Nature* 460: 103–107.
12. Wang, R., C. P. Dillon, L. Z. Shi, S. Milasta, R. Carter, D. Finkelstein, L. L. McCormick, P. Fitzgerald, H. Chi, J. Munger, and D. R. Green. 2011. The transcription factor Myc controls metabolic reprogramming upon T lymphocyte activation. *Immunity* 35: 871–882.
13. Wang, R., and D. R. Green. 2012. Metabolic checkpoints in activated T cells. *Nat. Immunol.* 13: 907–915.
14. Raud, B., D. G. Roy, A. S. Divakaruni, T. N. Tarasenko, R. Franke, E. H. Ma, B. Samborska, W. Y. Hsieh, A. H. Wong, P. Stuve, et al. 2018. Etomoxir actions on regulatory and memory T cells are independent of cpt1a-mediated fatty acid oxidation. *Cell Metab.* 28: 504–515.e7.
15. Berger, J. H., M. J. Charron, and D. L. Silver. 2012. Major facilitator superfamily domain-containing protein 2a (MFSD2A) has roles in body growth, motor function, and lipid metabolism. *PLoS One* 7: e50629.
16. Nguyen, L. N., D. Ma, G. Shui, P. Wong, A. Cazenave-Gassiot, X. Zhang, M. R. Wenk, E. L. Goh, and D. L. Silver. 2014. Mfsd2a is a transporter for the essential omega-3 fatty acid docosahexaenoic acid. *Nature* 509: 503–506.
17. Wong, B. H., J. P. Chan, A. Cazenave-Gassiot, R. W. Poh, J. C. Foo, D. L. Galam, S. Ghosh, L. N. Nguyen, V. A. Barathi, S. W. Yeo, et al. 2016. Mfsd2a is a transporter for the essential ω-3 fatty acid docosahexaenoic acid (DHA) in eye and is important for photoreceptor cell development. *J. Biol. Chem.* 291: 10501–10514.
18. Alakbarzade, V., A. Hameed, D. Q. Quek, B. A. Chioza, E. L. Baple, A. Cazenave-Gassiot, L. N. Nguyen, M. R. Wenk, A. Q. Ahmad, A. Sreekantan-Nair, et al. 2015. A partially inactivating mutation in the sodium-dependent lysophosphatidylcholine transporter MFSD2A causes a non-lethal microcephaly syndrome. *Nat. Genet.* 47: 814–817.
19. Guemez-Gamboa, A., L. N. Nguyen, H. Yang, M. S. Zaki, M. Kara, T. Ben-Omran, N. Akizu, R. O. Rosti, B. Rosti, E. Scott, et al. 2015. Inactivating mutations in MFSD2A, required for omega-3 fatty acid transport in brain, cause a lethal microcephaly syndrome. *Nat. Genet.* 47: 809–813.
20. Harel, T., D. Q. Y. Quek, B. H. Wong, A. Cazenave-Gassiot, M. R. Wenk, H. Fan, I. Berger, D. Shmueli, A. Shaag, D. L. Silver, et al. 2018. Homozygous

Downloaded from http://www.jimmunol.org/ by guest on February 24, 2022

mutation in MFSD2A, encoding a lysolipid transporter for docosahexanoic acid, is associated with microcephaly and hypomyelination. *Neurogenetics* 19: 227–235.
21. Chan, J. P., B. H. Wong, C. F. Chin, D. L. A. Galam, J. C. Foo, L. C. Wong, S. Ghosh, M. R. Wenk, A. Cazenave-Gassiot, and D. L. Silver. 2018. The lysolipid transporter Mfsd2a regulates lipogenesis in the developing brain. *PLoS Biol.* 16: e2006443.
22. Boggs, K. P., C. O. Rock, and S. Jackowski. 1995. Lysophosphatidylcholine and 1-O-octadecyl-2-O-methyl-rac-glycero-3-phosphocholine inhibit the CDP-choline pathway of phosphatidylcholine synthesis at the CTP:phosphocholine cytidylyltransferase step. *J. Biol. Chem.* 270: 7757–7764.
23. Gauster, M., G. Rechberger, A. Sovic, G. Hörl, E. Steyrer, W. Sattler, and S. Frank. 2005. Endothelial lipase releases saturated and unsaturated fatty acids of high density lipoprotein phosphatidylcholine. *J. Lipid Res.* 46: 1517–1525.
24. Schmitz, G., and K. Ruebsaamen. 2010. Metabolism and atherogenic disease association of lysophosphatidylcholine. *Atherosclerosis* 208: 10–18.
25. Vance, D. E. 2008. Role of phosphatidylcholine biosynthesis in the regulation of lipoprotein homeostasis. *Curr. Opin. Lipidol.* 19: 229–234.
26. Fox, C. J., P. S. Hammerman, and C. B. Thompson. 2005. Fuel feeds function: energy metabolism and the T-cell response. *Nat. Rev. Immunol.* 5: 844–852.
27. Wofford, J. A., H. L. Wieman, S. R. Jacobs, Y. Zhao, and J. C. Rathmell. 2008. IL-7 promotes Glut1 trafficking and glucose uptake via STAT5-mediated activation of Akt to support T-cell survival. *Blood* 111: 2101–2111.
28. de Jong, A. J., M. Kloppenburg, R. E. Toes, and A. Ioan-Facsinay. 2014. Fatty acids, lipid mediators, and T-cell function. *Front. Immunol.* 5: 483.
29. Hara, Y., Y. Kusumi, M. Mitsumata, X. K. Li, and M. Fujino. 2008. Lysophosphatidylcholine upregulates LOX-1, chemokine receptors, and activation-related transcription factors in human T-cell line Jurkat. *J. Thromb. Thrombolysis* 26: 113–118.
30. Nishi, E., N. Kume, H. Ochi, H. Moriwaki, Y. Wakatsuki, S. Higashiyama, N. Taniguchi, and T. Kita. 1997. Lysophosphatidylcholine increases expression of heparin-binding epidermal growth factor-like growth factor in human T lymphocytes. *Circ. Res.* 80: 638–644.
31. Nishi, E., N. Kume, Y. Ueno, H. Ochi, H. Moriwaki, and T. Kita. 1998. Lysophosphatidylcholine enhances cytokine-induced interferon gamma expression in human T lymphocytes. *Circ. Res.* 83: 508–515.
32. Smith, P. M., M. R. Howitt, N. Panikov, M. Michaud, C. A. Gallini, M. Bohlooly-Y, J. N. Glickman, and W. S. Garrett. 2013. The microbial metabolites, short-chain fatty acids, regulate colonic Treg cell homeostasis. *Science* 341: 569–573.
33. Meyer zu Heringdorf, D., and K. H. Jakobs. 2007. Lysophospholipid receptors: signalling, pharmacology and regulation by lysophospholipid metabolism. *Biochim. Biophys. Acta* 1768: 923–940.
34. Soga, T., T. Ohishi, T. Matsui, T. Saito, M. Matsumoto, J. Takasaki, S. Matsumoto, M. Kamohara, H. Hiyama, S. Yoshida, et al. 2005. Lysophosphatidylcholine enhances glucose-dependent insulin secretion via an orphan G-protein-coupled receptor. *Biochem. Biophys. Res. Commun.* 326: 744–751.
35. Fagone, P., and S. Jackowski. 2009. Membrane phospholipid synthesis and endoplasmic reticulum function. *J. Lipid Res.* 50(Suppl.): S311–S316.
36. van der Windt, G. J., B. Everts, C. H. Chang, J. D. Curtis, T. C. Freitas, E. Amiel, E. J. Pearce, and E. L. Pearce. 2012. Mitochondrial respiratory capacity is a critical regulator of CD8+ T cell memory development. *Immunity* 36: 68–78.
37. van der Windt, G. J., D. O'Sullivan, B. Everts, S. C. Huang, M. D. Buck, J. D. Curtis, C. H. Chang, A. M. Smith, T. Ai, B. Faubert, et al. 2013. CD8 memory T cells have a bioenergetic advantage that underlies their rapid recall ability. *Proc. Natl. Acad. Sci. USA* 110: 14336–14341.
38. Ibitokou, S. A., B. E. Dillon, M. Sinha, B. Szczesny, A. Delgadillo, D. Reda Abdelrahman, C. Szabo, L. Abu-Elheiga, C. Porter, D. Tuvdendorj, and R. Stephens. 2018. Early inhibition of fatty acid synthesis reduces generation of memory precursor effector T cells in chronic infection. *J. Immunol.* 200: 643–656.
39. Ben-Zvi, A., B. Lacoste, E. Kur, B. J. Andreone, Y. Mayshar, H. Yan, and C. Gu. 2014. Mfsd2a is critical for the formation and function of the blood-brain barrier. *Nature* 509: 507–511.
40. Chang, C. H., J. D. Curtis, L. B. Maggi, Jr., B. Faubert, A. V. Villarino, D. O'Sullivan, S. C. Huang, G. J. van der Windt, J. Blagih, J. Qiu, et al. 2013. Posttranscriptional control of T cell effector function by aerobic glycolysis. *Cell* 153: 1239–1251.

Downloaded from http://www.jimmunol.org/ by guest on February 24, 2022